

Polydopamine/Ethylenediamine Nanoparticles Embedding a Photosynthetic Bacterial Reaction Center for Efficient Photocurrent Generation

Gabriella Buscemi, Danilo Vona, Roberta Ragni, Roberto Comparelli, Massimo Trotta,*
Francesco Milano,* and Gianluca Maria Farinola*

Photoactive biohybrid soft nanoparticles are obtained by embedding the *Rhodospira rubra* Reaction Center (RC) in polydopamine (PDA) suspended aggregates and treating them with ethylenediamine (EDA). Such PDA:EDA@RC nanoparticles are investigated for photocurrent generation in photoelectrochemical cells, which are able to convert sunlight into electrical energy. The photosynthetic protein retains its structural and functional integrity in the nanostructures and the PDA:EDA@RC nanoparticles exhibit better water dispersity, improved light collection ability, and higher photocurrent generation compared to the PDA@RC precursors, where the reaction center is embedded in pure PDA. The hybrid soft nanoparticles incorporating the RC bacterial photoenzyme show charge separated state generation comparable to that of the pristine enzyme in solution, overcoming the main limitation of RC encapsulation in pure PDA, which is the polymer low light transmission ability. As a consequence, photocurrents obtained by RC within the PDA:EDA environment are almost doubled with respect to the PDA@RC. The biohybrid composites described here represent an interesting example of effective functional nanostructures for sunlight photoconversion based on a biological component addressed in a tunable biocompatible polymer composite, also showing the potential of fine chemical tailoring of polydopamine biointerfaces.

1. Introduction

Biohybrid nanostructures based on photoenzymes from photosynthetic organisms, which are able to efficiently convert solar light into charge separated states, open up new concepts in the design of sustainable systems for solar energy conversion.^[1]

In particular, bacterial reaction centers (RC), such as the RC obtained from the purple photosynthetic bacterium *Rhodospira rubra* (*R. rubra*), have raised interest for these applications since they are easy to isolate and purify and they can be handled outside their native environment without loss of functionality.^[2]

More in detail, the bacterial RC as the one used in this study^[3] is a membrane spanning protein composed of three subunits non-covalently bound to a series of cofactors arranged in two symmetrical branches A and B (Figure 1).

Upon photoexcitation, a dimer (D) of bacteriochlorophylls absorbing at 865 nm transfers, with remarkable unitary


quantum yield, an electron along the A branch to a bacteriochlorophyll (absorbing at 800 nm), then to a bacteriopheophytin (absorbing at 760 nm) and finally to the so-called quinone acceptor complex composed of two ubiquinone-10 (UQ₁₀) molecules located in the Q_A and Q_B pockets, respectively. The ratio of the band absorbance at 760, 800 and 865 nm is 1:2:1 in the intact protein. The final charge separated state (either D⁺Q_B⁻ or D⁺Q_A⁻ if the Q_B site is blocked or empty) has deep absorption minimum at 865 nm in the light-dark difference spectrum suitable to study the protein photoactivity. In the presence of the physiological electron donor cytochrome c₂, or artificial donors such as ferrocene and derivatives, RC photoactivation leads to a fully reduced and fully protonated UQ₁₀H₂ molecule at the Q_B site, that leaves the pocket and can be replaced by another UQ₁₀ or analogous ubiquinone molecules present in solution. Such photocycle is often exploited in photoelectrochemical cells,^[1b,5] capable to convert sunlight into electrical energy, recently reaching a record of 1.3 mA cm⁻² in hybrid systems involving transition metal–semiconductor Schottky junctions.^[6]

The photocycle can be reproduced using isolated RC suspended in direct,^[2a,7] or inverse micellar systems,^[8] but it can

Dr. G. Buscemi, Dr. D. Vona, Dr. R. Ragni, Prof. G. M. Farinola
Chemistry Department
University of Bari "Aldo Moro"
via Orabona 4, Bari I-70126, Italy
E-mail: gianlucamaria.farinola@uniba.it

Dr. R. Comparelli, Dr. M. Trotta
CNR-IPCF
Istituto per i Processi Chimico Fisici/Consiglio Nazionale delle Ricerche
via Orabona 4, Bari I-70126, Italy
E-mail: massimo.trotta@cnr.it

Dr. F. Milano
CNR-ISPA
Institute of Sciences of Food Production
S. P. Lecce-Monteroni, Lecce I-73100
E-mail: francesco.milano@cnr.it

 The ORCID identification number(s) for the author(s) of this article can be found under <https://doi.org/10.1002/adsu.202000303>.

© 2021 The Authors. Advanced Sustainable Systems published by Wiley-VCH GmbH. This is an open access article under the terms of the Creative Commons Attribution License, which permits use, distribution and reproduction in any medium, provided the original work is properly cited.

DOI: 10.1002/adsu.202000303

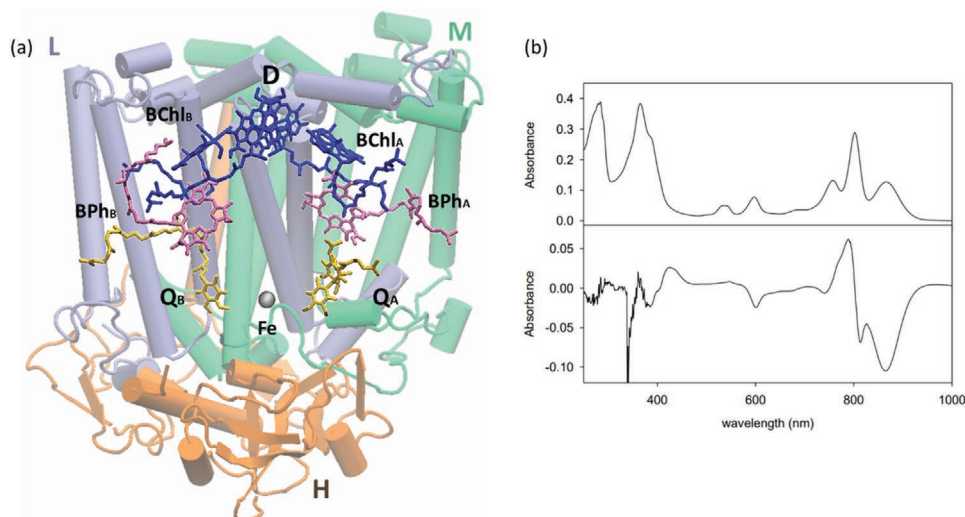


Figure 1. a) Protein and cofactors spatial arrangement obtained by crystallography (Protein Data Bank deposit code 2j8c^[4]); b) Absorption spectrum of detergent-solubilized RCs (upper panel) and light-dark spectrum, recorded under continuous saturating light ($\lambda < 400$ nm; lower panel).

also be used embedded and protected in biomimetic environments such as liposomes^[9] and giant vesicles,^[10] or in nonconventional solvents.^[11]

Beyond energy conversion applications, RC and other photoenzymes have been exploited for different applications such as charge storage devices,^[12] and electronic skins acting as tactile and UV sensors.^[13]

Among the systems for embedding functional RC molecules, we have explored polydopamine (PDA) for its many attracting features.^[14]

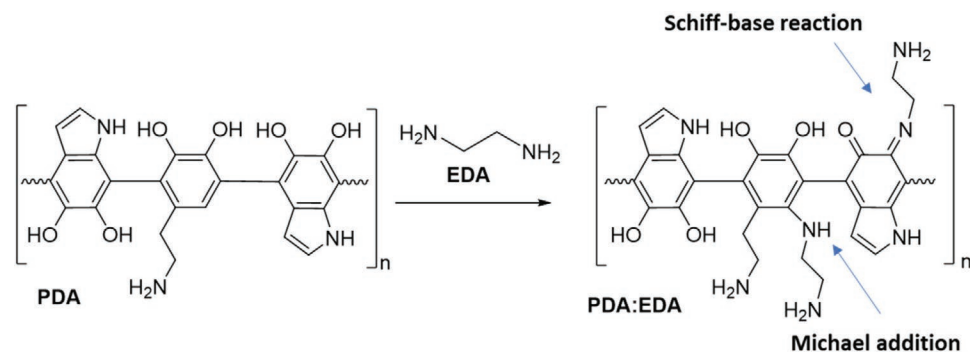
Polydopamine (PDA) is a melanin-like adhesive material deriving from the spontaneous oxidative polymerization of dopamine (DA) in mild basic oxygenated aqueous solutions.^[15] PDA is based on 5,6-dihydroxy-indole repeating units and π - π stacking of dopamine monomers, but its chemical structure is very complex and not yet fully elucidated.^[15a] One of the reasons of interest for PDA is due to its extraordinary ability to easily form biocompatible, stable, adhesive films with tunable thickness on a large variety of both hydrophobic and hydrophilic substrates.^[16] Moreover, further chemical modifications can be carried out using the hydroxyl and amino functional groups on PDA film surface. PDA has been also reported as a promising precursor of a large variety of materials including nanospheres grown around sacrificial templates,^[17] used to immobilize

enzymes and cells and protect them from surrounding environment. Interestingly, PDA not only forms surface adhered films, but also solution suspended nanoparticles (NPs) whose diameter can be controlled tuning DA polymerization conditions such as pH, temperature and monomer concentration.^[18] Like in films, also PDA NPs surface can be further modified via metal coordination, electrostatic interactions, covalent or hydrogen bonding, π - π stacking,^[19] for a variety of applications ranging from biomedicine to sensing.^[20]

However, PDA NPs are subjected to sedimentation and show optical opalescence and a dark color due to strong light absorption. All these drawbacks can limit their use, especially when light is used to trigger the desired function of systems based on a (bio)active species embedded in or coupled with PDA NPs.

Recently, a treatment with ethylenediamine (EDA) has been shown to induce a controlled degradation of PDA, promoting NPs size reduction and significant changes of their absorption and emission properties.^[21] In fact, EDA can convert some diketo-forms of the dihydroxy-indole units of PDA in Schiff bases functionalities, and it can react via Michael-like addition with some catechol rings,^[22] thus disrupting PDA nanostructure by interfering with π - π stacking between the aggregate polymeric chains (Scheme 1).

Compared to the pristine polymer, the resulting product exhibits improved water dispersibility and photoluminescence



Scheme 1. Schematic drawing of the reaction between EDA and PDA.

due to particles size reduction. Furthermore, PDA:EDA nanoparticles retain the biocompatibility of PDA, and remain suitable to interface biological components.^[21]

In our recent work,^[14] we reported a straightforward strategy to embed the photosynthetic reaction center (RC) from *R. sphaeroides* in PDA films deposited onto ITO electrode. By simultaneous one pot PDA polymerization and encapsulation of fully active protein, we reported a photoelectrode based on the bacterial RC immobilized in a much easier and effective way than most of the previously reported methods. Besides the formation of PDA films with embedded RC, (PDA@RC) film, we also observed that PDA generates colloidal nanoaggregates incorporating RC molecules and, in appropriate conditions, the protein is entrapped without loss of functionality.

The issue of high scattering and dark color of PDA@RC nanoparticles prompted us to explore the possibility to perform their controlled degradation with EDA treatment. Considering that the RC photoactivity depends on light harvesting,^[23] we expected that the decrease of PDA@RC suspension turbidity by EDA would have effectively enhanced the function of the confined protein.

Starting with the above described background, our study has led to building soft hybrid nanostructures based on PDA:EDA composites incorporating the bacterial RC and to testing their photoconversion ability in photoelectrochemical cells. The investigation has been performed assessing the following points: a) the effective size reduction and turbidity decrease of the PDA@RC nanoparticles upon EDA treatment without losses of encapsulated protein in the PDA:EDA@RC product;

b) the biocompatibility of the reaction towards RC structural integrity and functionality; c) the positive impact on the RC light collecting capability and photoactivity (including photocurrent generation) by the improved optical features of the modified polymer.

Our investigation has led to show that PDA:EDA@RC NPs are an interesting biohybrid system for solar energy conversion. Moreover, we envisage that the strategy adopted in this work could be applied also to different protein classes, paving the way to new routes for tailoring PDA nanoparticles as biocompatible carriers for biomacromolecules.

2. Results and Discussion

2.1. Preparation and Photophysical Characterization of PDA, PDA@RC, PDA:EDA, PDA:EDA@RC Nanoparticles

Nanoparticles of PDA and PDA@RC were prepared as detailed in the Experimental Section. As shown in Figure S1, all RC was embedded in PDA nanoparticles. EDA was added at different concentrations (1 – 500 mM) to both PDA and PDA@RC samples to produce a series of PDA:EDA and PDA:EDA@RC nanoparticles with reduced size versus their precursors. In fact, EDA was reported to interfere with the π - π stacking of PDA chains, partially disrupting the polymeric cross-linking, and eventually tuning its photophysical properties such as light absorption and emission.

Figure 2 shows the pictures and UV-vis-NIR absorption spectra of all stages (crude mixture, supernatant and

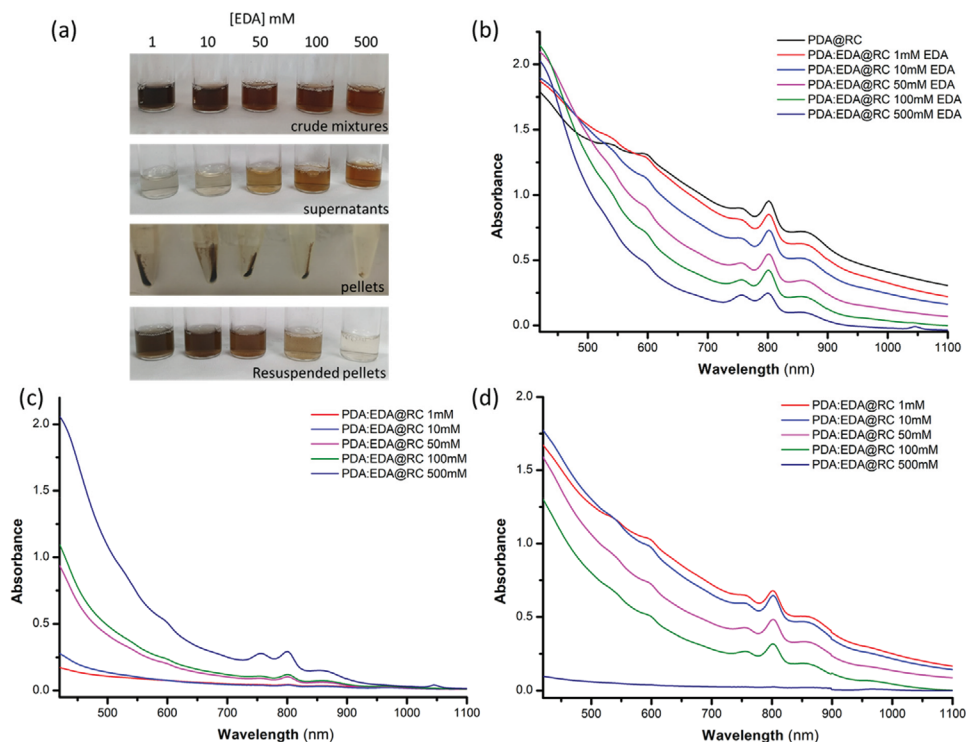


Figure 2. a) Stages of the reactions between EDA and PDA@RC at increasing EDA concentration; UV-vis-NIR absorption spectra of b) crude mixture, c) supernatant, and d) resuspended pellet of PDA@RC treated with increasing EDA concentration. All samples are in T_{25} pH 8.8 and with a starting RC concentration in PDA@RC of $1 \mu\text{M}$.

resuspended pellet) of the different reactions between PDA@RC and EDA at increasing concentration. Figure S2 shows the scattering corrected spectra, vertically stacked for better readability, allowing to better judge the NIR peaks relative amplitude. Figure 2a shows that increasing the EDA concentration, a reduction of the dark color of crude mixtures and resuspended pellet is observed, while an opposite trend occurs in the supernatant. The centrifugation at $5000 \times g$ allows to isolate different amounts of pellet depending on EDA concentration; in fact, EDA reduces particle sizes influencing their distributions in the pellet and supernatant. Increasing the EDA concentration and working at the same centrifugation conditions, the amount of pellet is gradually decreased (Figure 2a). The UV-vis-NIR absorption spectra of crude mixtures (Figure 2b and Figure S2a) can be regarded as the result of combination of various light absorption contributions from: RC (mainly in the 760–900 nm range), PDA (whose absorption is nearly constant in the investigated range), the EDA induced modification of PDA nanostructure (more evident below 600 nm and proportional to the EDA concentration) and light scattering (inversely proportional to the EDA concentration) occurring in all suspensions. The presence of an isosbestic-like region in the 450–500 nm range further confirms a conversion of the dark grey PDA polymer to a reddish PDA:EDA reaction product, whose contribution to absorption differs from that of bare EDA in solution (Figure S3). Figure 2c, relevant to supernatants, shows much lower scattering and negligible presence of RC in all samples with the exception for the 500 mM EDA derived sample. Figure S2b evidences how treatment with 500 mM EDA induces a partial denaturation of RC as the bands in the NIR region are no longer in the optimal 1:2:1 ratio. Moreover, light absorption below 600 nm, increasing with EDA concentration, indicates that supernatants are rich of PDA:EDA small nanoparticles, deriving from partial PDA degradation, that do not precipitate under the selected centrifugation conditions. According to the literature,^[21] we also found that nanoparticles in supernatants obtained by treatment with EDA are photoluminescent, with emission peaks tunable with EDA concentration (1–500 mM) in the 495–565 nm range (Figure S4).

Figure 2d shows that light scattering in the resuspended pellets is slightly lower than the corresponding crude mixtures, while light absorption below 600 nm is significantly reduced, as expected considering that small PDA:EDA reddish nanoparticles are mainly present in the supernatant. Resuspended pellets include almost entirely the RCs (90–96%) up to the 100 mM EDA treated sample, while at 500 mM EDA, all the protein remains in the supernatant, likely embedded in PDA:EDA nanoparticles that are too small to be precipitated upon centrifugation. Figure S2c confirms that in all samples treated with up to 100 mM EDA the RCs retain their structural integrity.

2.2. Morphological Characterization of Nanoparticles by DLS and SEM

We selected 100 mM as the optimal EDA concentration leading to PDA:EDA@RC nanoparticles with the lowest scattering contribution and the highest RC content preserving its structural integrity. The morphological characterization was performed

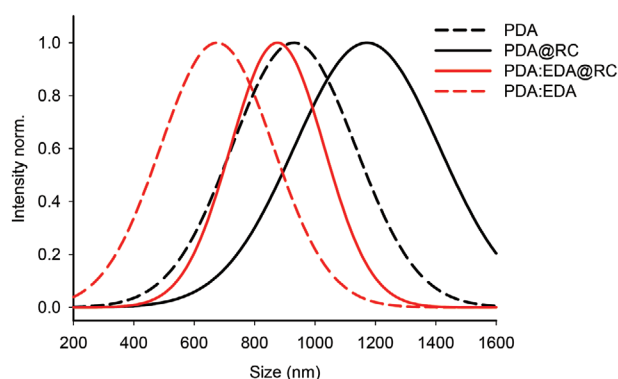


Figure 3. Hydrodynamic diameter distributions obtained by DLS for PDA, PDA:EDA, PDA@RC, PDA:EDA@RC recorded at 25°C. All samples are in T_{25} pH 8.8 and with 1 μ M RC.

by both dynamic light scattering (DLS) and scanning electron microscopy (SEM) measurements.

Figure 3 shows DLS size distributions of bare PDA, PDA:EDA, PDA@RC and PDA:EDA@RC, dispersed in T_{25} . An increase of the particles average size is observed, passing from 930 ± 200 for bare PDA to 1170 ± 240 for PDA@RC particles. After 100 mM EDA treatment, all the hydrodynamic diameters decrease, with average size values set at 670 ± 180 for PDA:EDA and 870 ± 150 for PDA:EDA@RC. These results are in agreement with those expected considering the relevant absorption spectra (Figure S5), since the characteristic increase of absorbance upon decrease of wavelengths is more evident for PDA@RC than for PDA, whereas a less evident difference is observed in absorption spectra of PDA:EDA@RC and PDA:EDA.

SEM micrographs of PDA (Figure 4a) and PDA:EDA (Figure 4b) show an evident decrease (from 500 ± 100 nm to 350 ± 100 nm) of the average size after EDA treatment. Figure 4c shows that RC induces micrometric clusters in the PDA@RC sample (see arrow) responsible also for the higher hydrodynamic radius observed in the DLS measurement. The PDA:EDA@RC particles in Figure 4d exhibit reduced sizes with respect to PDA@RC and after deposition both nanoparticles and a film-like structure (see arrows) are visible. A statistical image analysis of the nanoparticles, after separation of the larger clusters, confirms a decrease of PDA@RC particles after the EDA treatment from 350 ± 100 to 160 ± 60 nm (p value < 0.05 by Anova validation).

2.3. Photoactivity Investigation of Embedded RC by Transient Absorption

Steady-state light-dark difference spectrum of PDA:EDA@RC from 100 mM EDA (RC 0.2 μ M and saturating excitation light with $\lambda < 400$ nm) shown in Figure 5a presents a pattern very similar to that recorded in detergent (Figure 1b, lower panel), confirming that the protein retains its normal photoactivity upon encapsulation. Transient absorption measurements (TA) were carried out to investigate the RC photoactivity in PDA@RC and PDA:EDA@RC samples (both for crude mixtures and resuspended pellets) obtained by treatment with EDA at different concentrations (1–500 mM). The amount of embedded RC that can

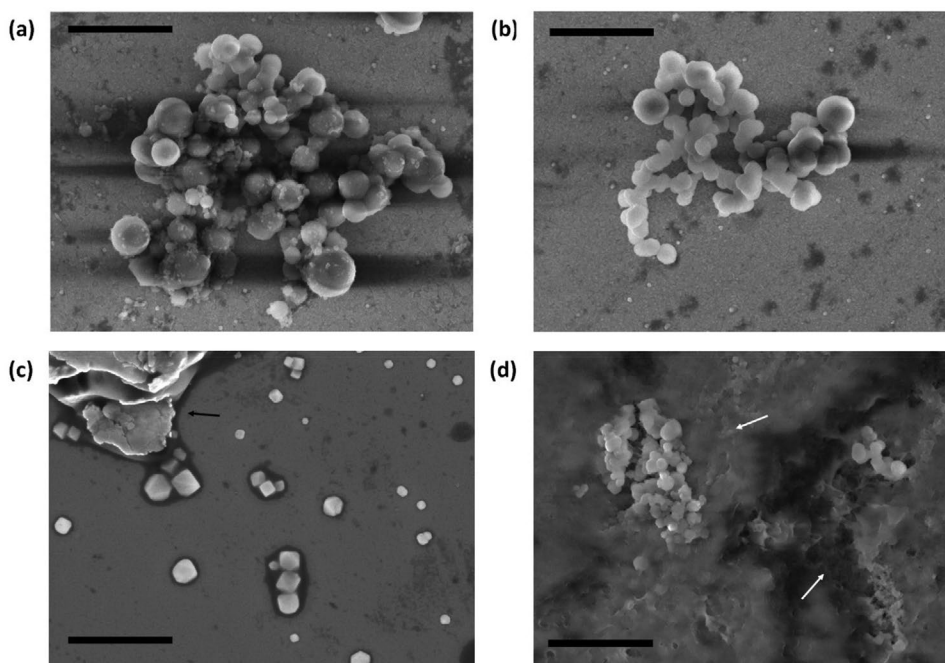


Figure 4. SEM images of a) PDA, b) PDA:EDA, c) PDA@RC (arrow: aggregates), and d) PDA:EDA@RC (arrows: film-like material). Scale bar: 2 μm .

be photoexcited is assessed monitoring the absorbance changes at 865 nm,^[24] where the band of the RC dimer is bleached upon formation of the charge separated state, as detailed in the

Experimental Section. Light intensity was set to a subsaturating value in order to excite about 40% of bare RC, with the aim to study the optical filtering effects of PDA and PDA:EDA coatings.

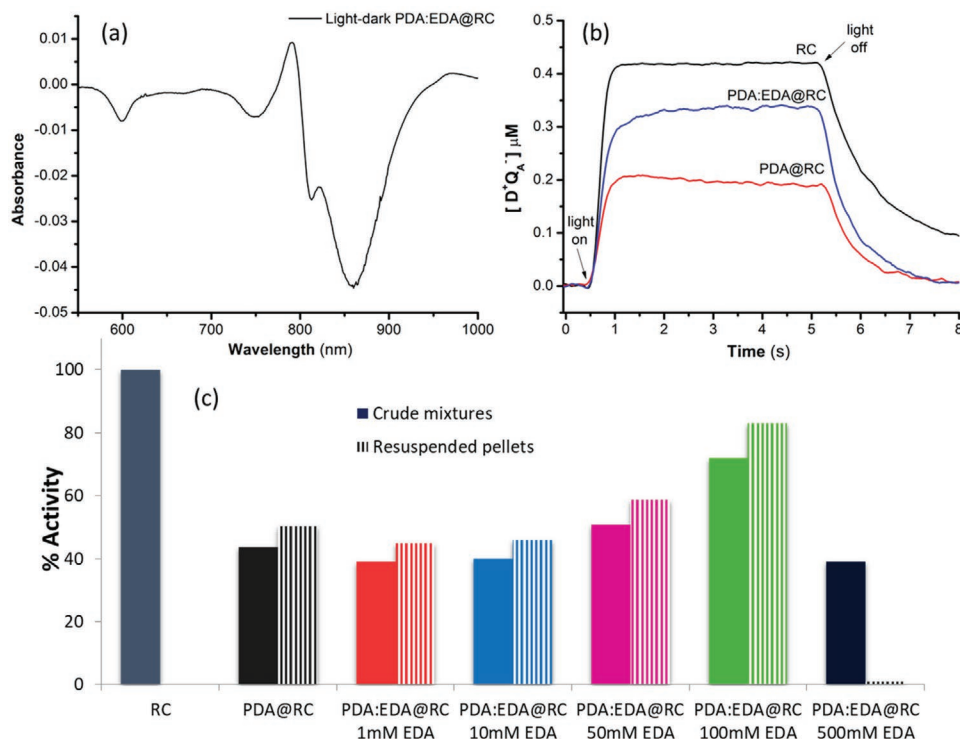


Figure 5. a) Light-dark difference spectrum of PDA:EDA@RC from 100 mM EDA (resuspended pellet) with RC 0.2 μM illuminated with UV ($\lambda < 400 \text{ nm}$) saturating light; b) Concentration of the charge separated state $D^+Q_A^-$ recorded at 865 nm obtained for RC, PDA@RC and PDA:EDA@RC from 100 mM EDA (resuspended pellets); c) histogram summarizing TA data for all PDA:EDA@RC samples (filled bar for crude mixtures, striped bar for resuspended pellets). Data refer to 1 μM RC illuminated by sub saturating white light (λ 350–600 nm).

Figure 5b refers to TA measurements for detergent-solubilized RC, and resuspended pellet of PDA@RC and PDA:EDA@RC from 100 mM EDA, while Figure 5c summarizes the experimental data of the complete series of samples, where the activity of detergent-solubilized RC was set as 100%. In PDA@RC, only 44% and 50% of RC can be photoexcited in crude mixture and in resuspended pellets, respectively. The higher photo-excitability of RC in resuspended pellets versus crude mixtures is also observed in all EDA treated samples. Moreover, as the EDA concentration increases, slight differences are noticed up to 10 mM EDA compared to unmodified PDA, while substantial improvements are obtained starting from 50 mM EDA reaching the maximum value of 83% photo-excitable RC at 100 mM EDA. These results can be rationalized considering the progressive decrease of suspension turbidity. Finally, at 500 mM EDA the photoactivity of RC in the crude mixture is reduced to 39% as a consequence of partial photoenzyme denaturation, while the resuspended pellet shows negligible photoactivity due to the lack of a significant amount of RC (Figure 2d).

2.4. Photocurrent Generation by PDA@RC and PDA:EDA@RC Nanoparticles

The ability of PDA@RC and PDA:EDA@RC to produce photocurrents has been explored. The photocycle in bacterial RC photoenzyme involves the reduction of ubiquinone-10 in the Q_B pocket to ubiquinol, that occurs with the simultaneous

oxidation of two cytochrome c^{2+} proteins. We used a photoelectrochemical cell (PEC) with a classical three-electrode configuration to measure the photocurrent generated in RC-based systems, using FcMeOH as organometallic electron donor instead of cytochrome and decylubiquinone (dQ) as electron acceptor in place of UQ₁₀, both having suitable redox potential and chemical reactivity.

Upon illumination a photocurrent can be recorded as the result of the reaction at the electrodes interface of light generated oxidated and reduced forms of mediators. Depending on the reaction that occurs at the WE, the photocurrent can be cathodic or anodic, with conventional negative or positive sign, respectively.^[25]

PDA@RC and PDA:EDA@RC (100 mM EDA) resuspended pellets were diluted to 0.14 μM RC final concentration, in 100 mM phosphate buffer with Triton X-100 at pH 7.0 (P₁₀₀TX_{0.03}).

The obtained photocurrents, recorded at the open circuit potential of -150 mV versus Ag/AgCl, are shown in Figure 6b. In our case, the negative sign of photocurrent indicates that a cathodic process is occurring at the WE, i.e., the reduction of FcMeOH⁺ photo-oxidized species, in agreement with the energetic diagram shown in Figure 6a. As an effect of EDA, the signal intensity is almost doubled from $\approx 0.7 \mu\text{A}/\text{cm}^2$ for PDA@RC to $\approx 1.3 \mu\text{A}/\text{cm}^2$ for PDA:EDA@RC. The increase of photocurrent is in agreement with the improved production of charge separated state of RC embedded in PDA:EDA (Figure 5b).

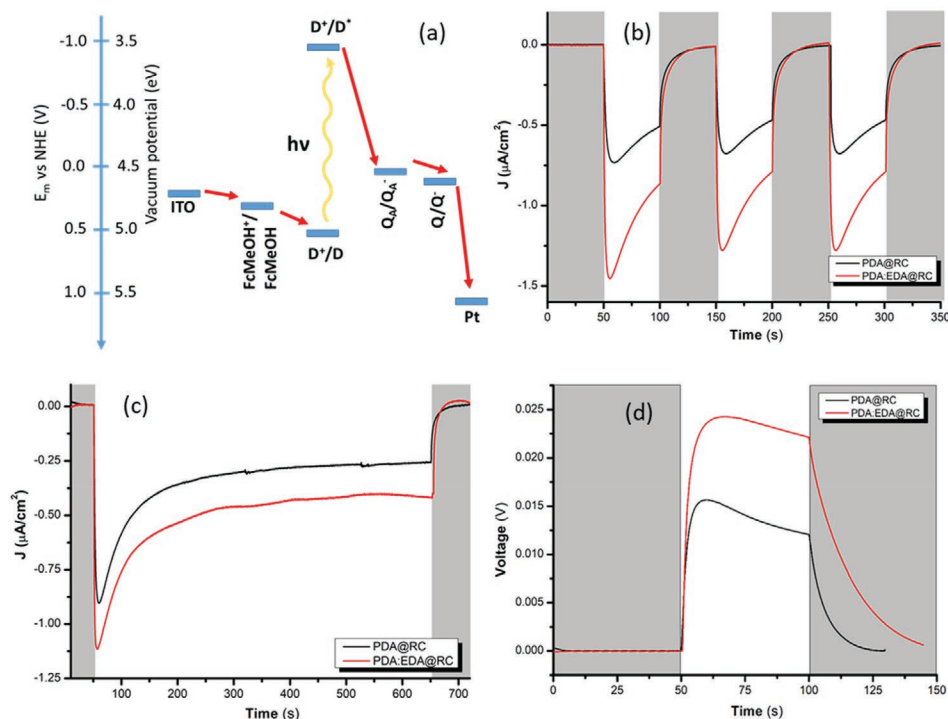


Figure 6. a) Diagram showing the energy levels (referred to both redox potential of normal hydrogen electrode (NHE) and to vacuum) of the species involved in the electrochemical cell. b) Photocurrents of 0.14 μM RC in PDA@RC and PDA:EDA@RC (100 mM EDA) in P₁₀₀TX_{0.03} pH 7.0, 0.3 mM FcMeOH, 0.1 mM dQ. c) Photocurrents as in (b) but with 10 min illumination time. d) Photo-chronopotentiometric measurement in two-electrode configuration for the same system. Illumination was provided by a 2.6 W LED emitting at 800 nm. All the solutions were kept in T₂₅ and diluted in P₁₀₀TX_{0.03} just before the electrochemical measurements.

Photocurrents, although decreasing to a significant extent within the first 5 min, remain stable after 10 min illumination time (Figure 6c) and it is reasonable to expect that can last for much longer, thanks to the efficient recycling of redox mediators at the electrodes. Moreover, after switching off the light, the current quickly reverts to the original baseline level, indicating that no long-term drifts or hysteresis effects are produced by the prolonged illumination. Finally, Figure 6d shows that the photovoltage obtained for PDA:EDA@RC, measured by photochronopotentiometry in two electrode configuration, is about 24 mV, again significantly higher than the value of 16 mV obtained with PDA@RC.

3. Conclusion

The effects of EDA on the morphology and photophysical properties of polydopamine nanoparticles embedding the *R. sphaeroides* bacterial photosynthetic Reaction center are presented. By tuning the EDA concentration, a controlled reduction of PDA particles size and a variation of their optical features was obtained. These changes affect the photoactivity of the encapsulated protein. More in detail, PDA:EDA@RC nanoparticles obtained by 100 mM EDA are characterized by higher water dispersity, photoactivity, and photocurrent generation compared to their PDA@RC precursors. PDA:EDA@RC appear hence intriguing soft bio-nanostructures for photocurrent generation in photoelectrochemical cells, and therefore interesting biohybrid models for solar energy conversion, whose properties can be finely tailored by varying the polymer composition. On a more general perspective, our study can be envisioned as an example of how chemical tuning of soft biohybrid structures can be an effective route to new systems for solar energy conversion based on photosynthetic components.

4. Experimental Section

Chemicals: The reagents for the phosphate buffer solutions, dQ, FcMeOH, Triton X-100 (TX), tris-(hydroxymethyl)-aminomethane (Tris), ethylenediamine and dopamine hydrochloride were purchased from Sigma. All aqueous solutions were prepared using water obtained by Milli-Q Gradient A-10 system (Millipore, 18.2 MΩ cm, organic carbon content ≤ 4 μg L⁻¹). ITO glass slides of 8 × 9 × 0.7 mm³ with ≈ 10 Ω sq⁻¹ surface resistivity and a transmittance >85% were washed in 5% Hellmanex solution, rinsed with bidistilled water and finally washed in acetone.

Preparation of RC: Reaction Centers were purified from the purple photosynthetic bacterium *R. sphaeroides* strain R26 following the procedure described by Isaacson.^[26] Protein purity is established by the absorbance ratio at 280 nm (A₂₈₀) and 802 nm (A₈₀₂), which was kept at A₂₈₀/A₈₀₂ < 1.4 while the absorbance ratio A₇₆₀/A₈₆₅ was kept ≤ 1. The ubiquinone content on average was about UQ₁₀/RC = 1.8.

Preparation of PDA and PDA@RC Nanoparticles: PDA nanoparticles were prepared dissolving dopamine hydrochloride 1.0 mg in 1 mL of Tris-HCl buffer (25 mM, pH 8.8) (T₂₅). The mixture was stirred at room temperature for 5 hours under atmospheric oxygen exposure to allow dopamine polymerization. A similar procedure was carried out for PDA@RC preparation except for the presence of RC 1 μM suspended in the T₂₅ buffer, and the reaction mixture was kept either in the dark or under green light to avoid protein light stress. PDA and PDA@RC nanoparticles were isolated as pellets by centrifugation at 5000 × g for 10 minutes and resuspended in T₂₅ buffer (1 mL).

Both polymerization reactions were monitored recording the UV-vis-NIR absorption spectra for: (i) the reaction mixture immediately after the addition of dopamine; (ii) the final reaction mixture after polymerization; (iii) the supernatant and (iv) the pellet after centrifugation.

Complete RC encapsulation into PDA was confirmed by the absence of the typical RC absorption peak at 802 nm in the supernatant.

Preparation of PDA:EDA and PDA:EDA@RC Nanoparticles: The PDA and PDA@RC pellets obtained according to the previously described procedure were suspended in 1 mL T₂₅ and ethylenediamine was added to obtain different concentrations (1, 10, 50, 100, 500 mM). The reaction mixtures were stirred overnight at room temperature under dark in a closed vial. PDA:EDA and PDA:EDA@RC nanoparticles were respectively pelleted by centrifugation at 5000 × g for 10 minutes and resuspended in T₂₅ buffer (1 mL).

RC concentration in PDA:EDA@RC is calculated by the characteristic absorption band at 802 nm ($\epsilon = 288 \pm 14 \text{ mM}^{-1} \text{ cm}^{-1}$) after the subtraction of the suspension scattering. For easier comparison, data are normalized to the protein concentration using the following equation:

$$\% \text{ RC}_{\text{pellet}} = \frac{A_i - A_f}{A_i} \cdot 100 \quad (1)$$

Where A_i is the absorbance at 802 nm of the reaction mixture before centrifugation, A_f is the absorbance at 802 nm of the resuspended pellet.

Scanning Electron Microscopy: For SEM analysis, ITO substrates (1 cm²) were washed twice in acetone and ethanol, sonicated and dried. The suspensions of PDA, PDA:EDA, PDA@RC and PDA:EDA@RC were deposited directly onto ITO substrates, dried overnight and dehydration was completed dipping the substrates in a series of fresh ethanol solutions. A Zeiss Sigma (Oberkochen, Germany) field emission and scanning electron microscope operating in the 0.5–20 KV range and equipped with a secondary electron detector and back diffusion was used for the characterization. Low accelerating voltage set to 5 KeV was exploited. Samples were mounted onto double sided carbon tape and grounded with silver paste. Image J software was used for average sizes calculations, and results were statistically evaluated via ANOVA.

Electrochemical Measurements: electrochemical measurements were performed with a three-electrode cell with an Autolab potentiostat PGSTAT 10. For the two-electrode configuration the reference electrode contact was short circuited with the counter electrode. The reference electrode was a micro Ag/AgCl electrode and the counter-electrode was Pt wire, while the working electrode (WE) was an ITO covered glass slide whose area immersed in the electrolytic solution was 0.7 cm². The support electrolyte was phosphate 100 mM, TX-100 0.03% pH 7.0 (P₁₀₀TX_{0.03}), supplemented with FcMeOH 300 μM as electron donor and dQ 100 μM as electron acceptor together with the PDA@RC and PDA:EDA@RC suspension. A bias of -0.15 V (corresponding to the OCV of the cell in the dark) was applied between the reference and the working electrodes. The light source for the photocurrent generation was a 2.6 W LED emitting at 800 nm providing an irradiance of 25 mW cm⁻². Light/dark cycles of 50 s were applied for repeated measurements or 10 min illumination for long-term functioning demonstration.

Equipment: Optical spectra in the range 350–1100 nm were recorded using a Cary 5000 UV-Vis-NIR spectrophotometer (Agilent Technologies Inc. – USA). Light-dark difference spectra have been obtained by illuminating the RC samples by means of Schott Karl Zeiss KL 1500 LCD Light Source equipped with a flexible light guide and 150 W QTH lamp filtered with a low-pass filter ($\lambda < 400 \text{ nm}$). Transient absorption measurements were performed using a kinetic spectrophotometer of local design,^[27] based on a 50 W QTH lamp, a Jobin Yvon H10 IR monochromator and a Hamamatsu R928 photomultiplier (Hamamatsu Photonics K.K., Hamamatsu City, Japan). A 250 W QTH lamp was used for continuous light excitation, placed at 90° with respect to the probe beam. A digital oscilloscope (Tektronix TKS3200) was used to collect the resulting data.

The percentage of RC embedded in PDA and PDA:EDA particles that can be photoactivated versus the bare RC, upon illumination with the

250 W QTH light source (filtered with a 350–600 bandpass filter), was calculated as it follows:

$$\% RC_{emb/bare} = \frac{\Delta ARC_{emb}}{\Delta ARC_{bare}} \cdot 100 \quad (2)$$

Where ΔA is evaluated at 865 nm and is proportional to the amount of $D^+Q_A^-$ charge separated state generated upon illumination.

Dynamic Light Scattering (DLS) measurements were performed with a Nanosizer ZS (Malvern instruments) for the determination of the size distribution of particles suspended in T_{25} . DLS measurements were performed in backscattering mode at pre-fixed detector angle.

Steady state Fluorescence emission spectra were obtained using a Varian Cary Eclipse fluorescence spectrophotometer (λ_{exc} 415 nm, excitation/emission slits 5/5).

Supporting Information

Supporting Information is available from the Wiley Online Library or from the author.

Acknowledgements

G.B. and D.V. contributed equally to this work. Funded by the European Union's Horizon 2020 Research and Innovation Programme under grant agreement No 800926 (HyPhOE, Hybrid Electronics Based on Photosynthetic Organisms), by PON MIUR project "Energy for TARANTO" (Grant no. ARS01_00637) and PRIN2017 (MUSSEL) Prot.2017JMPZN project.

Conflict of Interest

The authors declare no conflict of interest.

Data Availability Statement

Research data are not shared.

Keywords

biophotovoltaics, ethylenediamine-polydopamine materials, photocurrents, photosynthetic bacteria, polydopamine nanoparticles, reaction centers

Received: December 31, 2020

Revised: February 21, 2021

Published online: March 11, 2021

- [1] a) E. D. Glowacki, R. R. Tangorra, H. Coskun, D. Farka, A. Operamolla, Y. Kanbur, F. Milano, L. Giotta, G. M. Farinola, N. S. Sariciftci, *J. Mater. Chem. C* **2015**, *3*, 6554; b) F. Milano, A. Punzi, R. Ragni, M. Trotta, G. M. Farinola, *Adv. Funct. Mater.* **2019**, *29*, 1805521.
- [2] a) A. Agostiano, F. Milano, M. Trotta, *Eur. J. Biochem.* **1999**, *262*, 358; b) K. Hajdu, T. Szabó, A. E. Sarrai, L. Rinyu, L. Nagy, *Int. J. Photoenergy* **2017**, *2017*, 1.
- [3] a) G. Feher, J. P. Allen, M. Y. Okamura, D. C. Rees, *Nature* **1989**, *339*, 111; b) J. P. Allen, G. Feher, T. O. Yeates, H. Komiya, D. C. Rees,

- Proc. Natl. Acad. Sci. USA* **1988**, *85*, 8487; c) H. Komiya, T. O. Yeates, D. C. Rees, J. P. Allen, G. Feher, *Proc. Natl. Acad. Sci. USA* **1988**, *85*, 9012; d) T. O. Yeates, H. Komiya, A. Chirino, D. C. Rees, J. P. Allen, G. Feher, *Proc. Natl. Acad. Sci. USA* **1988**, *85*, 7993; e) A. Operamolla, R. Ragni, F. Milano, R. R. Tangorra, A. Antonucci, A. Agostiano, M. Trotta, G. M. Farinola, *J. Mater. Chem. C* **2015**, *3*, 6471.
- [4] J. Koepke, E.-M. Krammer, A. R. Kligen, P. Sebban, G. M. Ullmann, G. Fritzsche, *J. Mol. Biol.* **2007**, *371*, 396.
- [5] a) M. Di Lauro, S. la Gatta, C. A. Bortolotti, V. Beni, V. Parkula, S. Drakopoulou, M. Giordani, M. Berto, F. Milano, T. Cramer, M. Murgia, A. Agostiano, G. M. Farinola, M. Trotta, F. Biscarini, *Adv. Electron. Mater.* **2020**, *6*, 1900888; b) M. Di Lauro, G. Buscemi, M. Bianchi, A. De Salvo, M. Berto, S. Carli, G. M. Farinola, L. Fadiga, F. Biscarini, M. Trotta, *MRS Advances* **2020**, *5*, 985; c) S. M. Mirvakili, J. E. Slota, A. R. Usgaocar, A. Mahmoudzadeh, D. Jun, M. N. Mirvakili, J. T. Beatty, J. D. W. Madden, *Adv. Funct. Mater.* **2014**, *24*, 4789; d) A. Mahmoudzadeh, R. Saer, D. Jun, S. M. Mirvakili, A. Takshi, B. Iranpour, E. Ouellet, E. T. Lagally, J. D. W. Madden, J. T. Beatty, *Smart Mater. Struct.* **2011**, *20*, 094019.
- [6] S. K. Ravi, Y. Zhang, Y. Wang, D. K. Nandakumar, W. Sun, M. R. Jones, S. C. Tan, *Adv. Energy Mater.* **2019**, *9*, 1901449.
- [7] L. Gerencser, P. Maroti, *Biochemistry* **2006**, *45*, 5650.
- [8] A. Mallardi, G. Palazzo, G. Venturoli, *J. Phys. Chem. B* **1997**, *101*, 7850.
- [9] a) F. Milano, F. Italiano, A. Agostiano, M. Trotta, *Photosynth. Res.* **2009**, *100*, 107; b) E. Altamura, F. Milano, M. Trotta, P. Stano, F. Mavelli, in *Advances in Bionanomaterials*, Springer, Cham **2018**, p. 97; c) E. Altamura, R. Fiorentino, F. Milano, M. Trotta, G. Palazzo, P. Stano, F. Mavelli, *Biophys. Chem.* **2017**, *229*, 46.
- [10] E. Altamura, F. Milano, R. R. Tangorra, M. Trotta, O. H. Omar, P. Stano, F. Mavelli, *Proc. Natl. Acad. Sci. USA* **2017**, *114*, 3837.
- [11] F. Milano, L. Giotta, M. R. Guascito, A. Agostiano, S. Sblendorio, L. Valli, F. M. Perna, L. Cicco, M. Trotta, V. Capriati, *ACS Sustainable Chem. Eng.* **2017**, *5*, 7768.
- [12] S. K. Ravi, P. Rawding, A. M. Elshahawy, K. Huang, W. Sun, F. Zhao, J. Wang, M. R. Jones, S. C. Tan, *Nat. Commun.* **2019**, *10*, 902.
- [13] a) S. K. Ravi, N. Paul, L. Suresh, A. T. Salim, T. Wu, Z. Wu, M. R. Jones, S. C. Tan, *Mater. Horiz.* **2020**, *7*, 866; b) S. K. Ravi, T. Wu, V. S. Udayagiri, X. M. Vu, Y. Wang, M. R. Jones, S. C. Tan, *Adv. Mater.* **2018**, *30*, 1802290.
- [14] M. Lo Presti, M. M. Giangregorio, R. Ragni, L. Giotta, M. R. Guascito, R. Comparelli, E. Fanizza, R. R. Tangorra, A. Agostiano, M. Losurdo, G. M. Farinola, F. Milano, M. Trotta, *Adv. Electron. Mater.* **2020**, *6*, 2000140.
- [15] a) H. Lee, S. M. Dellatore, W. M. Miller, P. B. Messersmith, *Science* **2007**, *318*, 426; b) H. Lee, N. F. Scherer, P. B. Messersmith, *Proc. Natl. Acad. Sci. USA* **2006**, *103*, 12999; c) M. Sureshkumar, P.-N. Lee, C.-K. Lee, *J. Mater. Chem.* **2011**, *21*, 12316; d) Q. Wei, F. Zhang, J. Li, B. Li, C. Zhao, *Polym. Chem.* **2010**, *1*, 1430; e) Q. Ye, F. Zhou, W. Liu, *Chem. Soc. Rev.* **2011**, *40*, 4244; f) F. Bernsmann, A. Ponche, C. Ringwald, J. Hemmerlé, J. Raya, B. Bechinger, J. C. Voegel, P. Schaaf, V. Ball, *J. Phys. Chem. C* **2009**, *113*, 8234.
- [16] a) P. Palladino, F. Bettazzi, S. Scarano, *Anal. Bioanal. Chem.* **2019**, *411*, 4327; b) X. Wu, C. Yang, J. Ge, Z. Liu, *Nanoscale* **2015**, *7*, 18883; c) Y. Jiang, J. Zhai, L. Zhou, Y. He, L. Ma, J. Gao, *Biochem. Eng. J.* **2018**, *132*, 196; d) S. H. Yang, S. M. Kang, K.-B. Lee, T. D. Chung, H. Lee, I. S. Choi, *J. Am. Chem. Soc.* **2011**, *133*, 2795.
- [17] a) B. Yu, D. A. Wang, Q. Ye, F. Zhou, W. Liu, *Chem. Commun.* **2009**, <https://doi.org/10.1039/B910679K6789>; b) A. Postma, Y. Yan, Y. Wang, A. N. Zelikin, E. Tjijto, F. Caruso, *Chem. Mater.* **2009**, *21*, 3042.
- [18] a) V. Ball, *Frontiers in Bioengineering and Biotechnology* **2018**, *6*; b) F. Milano, M. Lopresti, D. Vona, G. Buscemi, M. Cantore, G. M. Farinola, M. Trotta, *MRS Advances* **2020**, *5*, 2299.

- [19] M. E. Lynge, R. van der Westen, A. Postma, B. Städler, *Nanoscale* **2011**, 3, 4916.
- [20] V. Ball, *Frontiers in Bioengineering and Biotechnology* **2018**, 6, 109.
- [21] G. E. Gu, C. S. Park, H.-J. Cho, T. H. Ha, J. Bae, O. S. Kwon, J.-S. Lee, C.-S. Lee, *Sci. Rep.* **2018**, 8, 4393.
- [22] a) M. Liu, J. Ji, X. Zhang, X. Zhang, B. Yang, F. Deng, Z. Li, K. Wang, Y. Yang, Y. Wei, *J. Mater. Chem. B* **2015**, 3, 3476; b) S. Harvey, D. Y. W. Ng, J. Szelwicka, L. Hueske, L. Veith, M. Raabe, I. Lieberwirth, G. Fytas, K. Wunderlich, T. Weil, *Biointerphases* **2018**, 13, 06D407; c) J. Liebscher, *Eur. J. Org. Chem.* **2019**, 2019, 4976; d) C. Zhao, F. Zuo, Z. Liao, Z. Qin, S. Du, Z. Zhao, *Macromol. Rapid Commun.* **2015**, 36, 909; e) M. L. Alfieri, L. Panzella, S. L. Oscurato, M. Salvatore, R. Avolio, M. E. Errico, P. Maddalena, A. Napolitano, V. Ball, M. d'Ischia, *Frontiers in Chemistry* **2019**, 7.
- [23] a) S. la Gatta, F. Milano, G. M. Farinola, A. Agostiano, M. Di Donato, A. Lapini, P. Foggi, M. Trotta, R. Ragni, *Biochim Biophys Acta Bioenerg* **2019**, 1860, 350; b) F. Milano, R. R. Tangorra, O. H. Omar, R. Ragni, A. Operamolla, A. Agostiano, G. M. Farinola, M. Trotta, *Angew. Chem.* **2012**, 124, 11181; c) O. Hassan Omar, S. la Gatta, R. R. Tangorra, F. Milano, R. Ragni, A. Operamolla, R. Argazzi, C. Chiorboli, A. Agostiano, M. Trotta, G. M. Farinola, *Bioconj. Chem.* **2016**, 27, 1614; d) C. Sissa, A. Painelli, F. Terenziani, M. Trotta, R. Ragni, *Phys. Chem. Chem. Phys.* **2020**, 22, 129; e) P. K. Dutta, S. Levenberg, A. Loskutov, D. Jun, R. Saer, J. T. Beatty, S. Lin, Y. Liu, N. W. Woodbury, H. Yan, *J. Am. Chem. Soc.* **2014**, 136, 16618.
- [24] U. Andréasson, L.-E. Andréasson, *Photosynth. Res.* **2003**, 75, 223.
- [25] F. Milano, F. Ciriaco, M. Trotta, D. Chirizzi, V. De Leo, A. Agostiano, L. Valli, L. Giotta, M. R. Guascito, *Electrochim. Acta* **2019**, 293, 105.
- [26] R. A. Isaacson, F. Lendzian, E. C. Abresch, W. Lubitz, G. Feher, *Biophys. J.* **1995**, 69, 311.
- [27] F. Milano, A. Agostiano, F. Mavelli, M. Trotta, *Eur. J. Biochem.* **2003**, 270, 4595.